Terahertz studies of 2D and 3D topological transitions

M. Marcinkiewicz, Frederic Teppe, Christophe Consejo, Nina Diakonova, Wilfried Desrat, Dominique Coquillat, Sandra Ruffenach, Wojciech Knap, N. N. Mikhailov, S. A. Dvoretskii, et al.

Journal of Physics: Conference Series **647** (2015) 012037 doi:10.1088/1742-6596/647/1/012037

Terahertz studies of 2D and 3D topological transitions

M Marcinkiewicz[1], F Teppe[1], C Consejo[1], N Dyakonova[1], W Desrat[1], D Coquillat[1], S Ruffenach[1], W Knap[1], N N Mikhailov[2], S A Dvoretskii[2], F Gonzalez-Posada[3], J-B Rodriguez[3] and E Tournié[3]

[1]L2C, UMR 5221 CNRS, Université Montpellier, GIS Teralab, 34095 Montpellier, France
[2]A.V. Rzhanov Institute of Semiconductor Physics, Siberian Branch, Russian Academy of Science, 630090 Novosibirsk, Russia
[3]IES, UMR 5214, Université Montpellier, 34000 Montpellier, France

E-mail: Michal.Marcinkiewicz@univ-montp2.fr

Abstract. We report terahertz measurements on bulk HgCdTe crystals at the semiconductor-to-semimetal topological transition and InAs/GaSb inverted band structure quantum well. We show that physical parameters of these narrow gap systems driven in specific topological phases can be efficiently extracted by means of terahertz photoconductivity studies.

1. Introduction

In the past years, the discovery of novel topological states of matter has attracted significant attention [1]. The most salient feature of such topological insulators (TIs) is that they have a full insulating gap in the bulk but gapless edge or surface states at boundaries. For two-dimensional (2D) TIs, the 1D edge hosts gapless spin-helical edge channels linearly crossing at a Dirac point [2], as was demonstrated experimentally in HgTe quantum wells (QWs) and InAs/GaSb broken gap QWs [3], whereas a 3D TI has protected spin-helical surface states usually with a Dirac cone-like dispersion [4]. Recently, such Dirac-type excitation has been extended to 3D, leading to the concept of Dirac semimetals [5]. These remarkable states have nontrivial topological properties without having a bulk band gap. Experiments on Na_3Bi and Cd_3As_2 have indeed successfully confirmed their Dirac semimetal character. Three-dimensional ultra-relativistic massless electrons have also been observed in bulk $Hg_{1-x}Cd_xTe$ (MCT) at the point of semiconductor-to-semimetal topological transition [6].

2. Band properties

2.1. InAs/GaSb

InAs, GaSb, AlSb and related semiconductor alloys form a family with a sufficient lattice match (6.1 Angstrom family [7]) for epitaxial growth without significant strains in grown structures. The structure considered in this work was a AlSb/GaSb/InAs/AlSb double layer QW with AlSb barriers. The characteristic feature of such systems is the alignment of bands of GaSb and InAs – the conduction band of InAs overlaps with the GaSb valence band. That system is referred to as Broken-Gap QW (BGQW). In InAs/GaSb BGQW, the energy of the valence band edge of

GaSb is higher (tens of meV) than the conduction band edge of InAs – the structure exhibits semimetallic behaviour. Hole and electron states at the interface are mixed. This hybridisation of the bands opens a small energy gap with inverted band structure.

InAs/GaSb QWs allow us to study many interesting physical phenomena, such as the Quantum Spin Hall Effect (QSHE) [8] or magnetic field-induced semimetal-to-semiconductor transition [9].

2.2. MCT

The $Hg_{1-x}Cd_xTe$ compounds are widely used in infrared optics because they provide an unprecedented degree of freedom in band gap tunability with x [10]. As the Cd composition increases, the energy gap increases from a negative value for pure HgTe to a positive one with CdTe. For $x > x_c$ MCT is a conventional semiconductor, where for $x < x_c$ the band gap is negative and the whole structure becomes a semimetal. The two distinct phases are not topologically equivalent, as characterized by a Z_2 topological invariant [11]. It means that for a critical Cd composition $x_c = 0.17$ the energy gap vanishes. At this point the system exhibits a Dirac cone-like dispersion relation.

3. Results

3.1. InAs/GaSb BGQW

The sample designed for this study consists of a 3 nm GaSb cap layer, two 50 nm AlSb barriers with 8 nm GaSb and 15 nm InAs layers between them. The structure was grown on an AlSb/GaSb superlattice buffer layer and a n-doped GaAs substrate. The sample was processed and multiple Hall bars were prepared for measurements. A picture of one of the Hall bars is shown in the inset of Fig.2.

To probe the carrier density, magnetotransport and photoconductivity measurements were performed. The results shown on Fig.1 were obtained at $T = 1.65$ K during illumination with a 292 GHz Schottky source. The photovoltage curve was obtained using lock-in technique – the beam was modulated mechanically with a chopper and signal was measured by lock-in. The THz radiation and lock-in technique revealed the Shubnikov - de Haas (SdH) oscillations at much weaker magnetic fields, compared to standard magnetotransport measurements. A cyclotron resonance peak was observed at $B = 0.37$ T, which points to an effective electron mass of $m^* = 0.035\ m_e$. Those results are in good agreement with previous results obtained on similar samples by transmission measurements, not presented in this work. The carrier concentration, estimated by SdH measurements, was $n = 5.7{\cdot}10^{11}$ cm^{-2}.

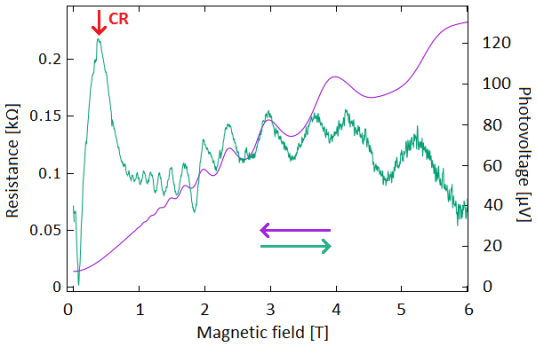

Figure 1. The photoconductivity of InAs/GaSb QW at 1.65 K and under illumination by 292 GHz radiation as a function of magnetic field. The red marker indicates the position of the cyclotron resonance. Purple line (left y axis) represents the standard magnetoresistance curve, measured for $I = 10$ μA. Teal line (right y axis) represents the photoconductivity curve.

Our sample does not have a gate – the only way to change the Fermi level position was to use the negative and positive persistent photoconductivity (NPPC and PPPC respectively) [12]. To probe the persistent photoconductivity effect, the sample was placed with an LED in liquid nitrogen (T = 77 K) and the conductivity of the sample was measured as a response to an illumination with red (blue) LED with peak wavelength λ = 660 (470) nm. The results, presented on Fig.2, are a sign of the PPPC effect. It was possible to increase the conductivity a few times before saturation was reached. The effect disappeared after warming up the sample to the room temperature.

The measurements were repeated in a liquid helium cryostat (T = 4.2 K). In contrast to measurements at T = 77K consecutive illuminations decreased the conductivity – the sample exhibited the NPPC effect. Those results are consistent with those obtained in [12], except that the change between PPPC and NPPC occurred at different temperature. PPPC and NPPC effects arise mainly from two competing mechanisms – PPPC occurs due to the creation of electron-hole pairs in InAs well and the capture of photoexcited holes by deep defects. On the other hand NPPC occurs due to the pumping of electrons into the local minima at the well-barrier interface, existing because of compositional fluctuations, which leads to decrease of electron concentration. The influence of those two processes changes with the temperature – in high temperatures PPPC effect dominates, in lower – NPPC. We claim that our system is different structurally and qualitatively, that is why the temperature range of PPPC and NPPC domination differs. More data are required to explain this dependence in a quantitative way.

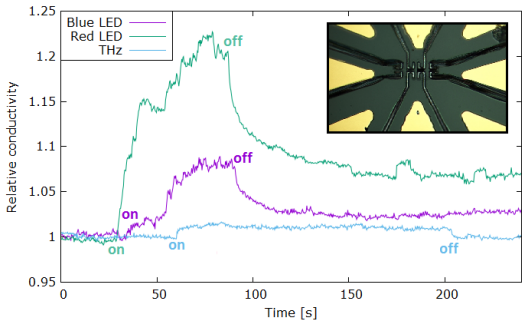

Figure 2. The results of illumination of the InAs/GaSb QW by blue and red LED light at T = 77 K. We observed an increased conductivity. This effect lasted after illumination was terminated. Light-blue curve presents change of conductivity while the sample was illuminated by THz light. In inset a photo of processed InAs/GaSb Hall bar is shown.

3.2. MCT bulk

A 3.2 μm thick MCT sample was grown using standard molecular-beam epitaxy on a 400 μm (013)-oriented semi-insulating GaAs substrate with a 50 nm thick ZnTe buffer layer and a 5 μm thick CdTe buffer layer. The cadmium concentration in the sample was x = 0.165. Therefore, an inverted band structure and a small negative gap are expected. The carrier density was estimated by magnetotransport and photoconductivity measurements.

THz induced SdH-like oscillations allow us to extract a carrier concentration of about $1 \cdot 10^{15}$ cm^{-3}, comparable to the electron concentration measured by Hall effect. Also, the amplitude of THz induced SdH oscillations changed with the temperature (Fig.3). Using Lifshitz-Kosevich formula [13] we were able to estimate the effective carrier mass in this sample (Fig.4).

The carrier effective mass found in sample A ($m^* = 2 \cdot 10^{-3}$ m_e) cannot be used to fit our results, but much higher mass values are necessary. The best fitting value is definitely $m^* = 2.1$ m_e, thus, three times higher than the larger heavy hole mass ever reported in this compound [10]. However, our experimental results are not accurate enough to validate this precise mass value and further experiments at lower temperatures have to be performed.

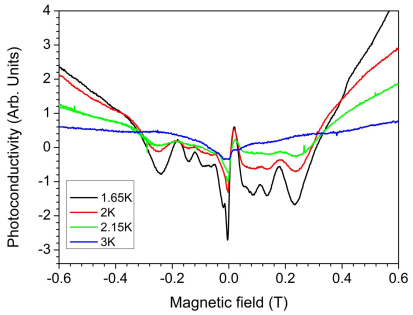

Figure 3. The close view of photoconductivity of bulk MCT sample B at 1.65 K under 292 GHz incident radiation as a function of magnetic field. Each line corresponds to a different temperature in range 1.65 K – 3 K. The rapid vanishing of the SdH oscillations with increasing temperature indicates that carriers have a relatively large effective mass.

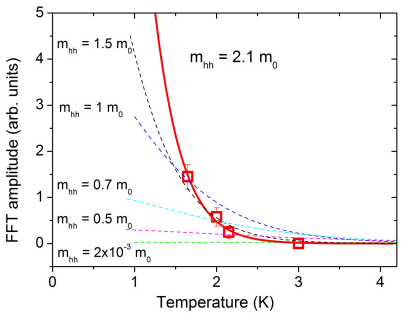

Figure 4. The amplitude of Fourier transform peaks corresponding to low field oscillations in MCT, as a function of temperature (empty squares). Dashed and straight lines are the fits for different values of effective mass.

4. Conclusion

We have studied by THz photoconductivity MCT bulk crystals and GaSb/InAs QW, which are known to exhibit semimetal-to-semiconductor topological phase transitions and Quantum Spin Hall Effect. Our first results allowed us to determine the heavy holes effective mass in MCT sample. In the case of GaSb/InAs QW , our THz photoconductivity results gave us information about the effective mass of electrons. We were also able, using PPPC and NPPC effect, to change the Fermi level in the structure, which is essential for future studies of topological phase transitions.

References

[1] Hasan G M Z and Kane C L 2010 *Rev. Mod. Phys.* **82** 3045-67
[2] König M et al 2007 *Science* **318** 766-70
[3] Halvorsen E, Galperin Y and Chao K A 2000 *Phys. Rev.* B **61** 16743
[4] Ando Y 2013 *J. Phys. Soc. Japn.* **82** 102001
[5] Young S M, Zaheer S, Teo J C Y, Kane C L, Mele E J and Rappe A M 2012 *Phys. Rev. Lett.* **108** 140405
[6] Bernevig B A, Hughes T L and Zhang S-C 2006 *Science* **314** 175761
[7] Kroemer H 2004 *Physica* E **20** 196-203
[8] Du L, Knez I, Sullivan G and Du R-R 2015 *Phys. Rev. Lett.* **114** 096802
[9] Lo Ikai and Mitchel W C 1993 *Phys. Rev.* B **48** 9118
[10] Rogalski A 2005 *Rep. Prog. Phys.* **68** 22672336
[11] Orlita M et al 2014 *Nature* **10** 233-38
[12] Wang W C, Tsai L C, Fan J C, Chen Y F and Lo Ikai 1999 *J. Appl. Phys.* **86** 3152
[13] Lifshitz I M and Kosevich A M 1955 *Zh. Eksp. Teor. Fiz.* **29** 730